

Structural and magnetic effect of bismuth substitution on Li-Co ferrite synthesized through microemulsion method

A. Saleem^a, M. S. Shifa^b, S. A. Buzdar^b, H. M. N. ul H. K. Asghar^c,
M. Mustaqeem^d, Z. A. Gilani^{c,*}, S. M. Ali^e, M. A. Sharf^f, A. K. Khan^g

^aDepartment of Physics, Government College University Faisalabad, Pakistan

^bInstitute of Physics, The Islamia University of Bahawalpur

^cDepartment of Physics, Balochistan University of Information Technology,
Engineering & Management Sciences, Quetta 87300, Pakistan

^dDepartment of Chemistry, National Taiwan University, No. 1, Section 4,
Roosevelt Road, Taipei 10617, Taiwan

^eDepartment of Physics and Astronomy, College of Science, P.O. BOX 2455, King
Saud University, Riyadh, 11451, Saudi Arabia

^fDepartment of Mechanical & Energy Systems Engineering, Faculty of
Engineering and Informatics, University of Bradford, Bradford BD7 1DP, United
Kingdom

^gDepartment of Physics, University of Central Punjab, Bahawalpur Campus,
Bahawalpur, Pakistan

Li-Co spinal ferrites were synthesized in pure and doped form by substituting/doping a post transition metal, bismuth in varying concentrations using micro-emulsion technique. Effect of bismuth substitution was studied by investigating the structural and magnetic properties in detail. X-ray diffractometer results confirmed the creation of single phase along with a slight occurrence of orthophase in prepared ferrites. Average crystallite size increased from 14 to 28 nm by increase in bismuth concentration. SEM micrographs were in complete agreement with XRD results showing spherical to cubic grains which was a confirmation of cubic spinal structure. Average estimated grain size of 52 nm showing agglomeration was also a good testimony of XRD results. VSM technique was employed to study magnetic properties of prepared samples within applied magnetic field strength of -10,000Oe to 10,000Oe. Ms and Hc values were observed to be decreasing with increasing bismuth content. Lower Ms and Hc values made our newly synthesized material fit for transformer cores and induction purposes.

(Received January 18, 2023; Accepted September 12, 2023)

Keywords: Li-Co, Bismuth, Nano-crystalline ferrites, Micro-emulsion, XRD, SEM, VSM

1. Introduction

Lithium base ferrites offer a wide range of potential uses owing their ease of synthesis and low cost. Li-ferrites have a good temperature stability of Ms which makes them a good commercial choice as a substituent of garnets in microwave devices. Most important applications of lithium base ferrites are in circulators, isolators, phase shifters, magnetic switching devices and microwave latching devices. The most common application of lithium ferrites is to be used as cathode in lithium batteries [1]. Spinel cubic structure of lithium base ferrites has polycrystalline structure with AB₂O₄ formula having octahedral(B) and tetrahedral(A) sites [2]. Introducing various dopants in varying proportions led to the formation of a versatile list of ferrites which show a diverse range of physical, morphologic and magnetic properties [3]. Furthermore, properties of synthesized material have a great influence of preparation technique [4]. A large number of researchers have adopted different synthesis routes like co-precipitation, sol-gel, microemulsion, oxalate precursor, ceramic and ball-milling method [5]. In present case of study,

* Corresponding author: zaheer.abbas@buitms.edu.pk
<https://doi.org/10.15251/JOR.2023.195.547>

microemulsion method is adopted as previous work of researchers showed a smallest grain size of ferrites in nano-scale. As smaller grain size implies larger surface to volume ratio that provides a huge range of atoms on surface. In this situation, a large electronic state determines the optoelectronic and electric properties of materials. Alongside preparation technique, choice of chemical composition, sintering temperature and PH values have a significant impact on microstructures. i.e., density, porosity, grain boundaries and grain sizes. Increase in PH causes a decrease in grain size which in addition leads to larger surface to volume ratio [6]. These parameters also controls the electrical, optical and magnetic properties of prepared materials [7].

In our present work, a series of bismuth doped lithium cobalt ferrites ($0.00 < x < 0.25$) has been made ready via microemulsion technique. One of the wet chemical synthesis techniques that limits the size of nano particles and it is easy and facile method. The sole purpose of research is to study the effect of dopant (bismuth) on the structural, morphological and magnetic properties of Li-Co ferrites and hence to determine the possibilities of using prepared material in high density, high frequency magnetic storage devices.

2. Experimental procedure

$\text{LiCo}_{0.5}\text{Bi}_x\text{Fe}_{2-x}\text{O}_4$ ($0.00 < x < 0.25$ with 0.05 steps) were prepared by novel micro-emulsion route. Bismuth (III) nitrate pentahydrate ($\text{Bi}(\text{NO}_3)_3 \cdot 5\text{H}_2\text{O}$ reagent grade, 98%, Sigma Aldrich), Cobalt (III) nitrate ($\text{Co}(\text{NO}_3)_3 \cdot 6\text{H}_2\text{O}$ analytical reagent, 98%, Sigma Aldrich), Lithium nitrate (LiNO_3 , 99.99% trace metal basis, Sigma Aldrich), Ferric nitrate nano hydrate ($\text{Fe}(\text{NO}_3)_3 \cdot 9\text{H}_2\text{O}$, reagent $\geq 98\%$, Sigma Aldrich), CTAB (Cetyltrimethylammonium bromide $\geq 99\%$ Sigma Aldrich) and Sodium hydroxide (NaOH , pellets, Sigma Aldrich) are the chemicals utilized.

Solutions of lithium, cobalt, bismuth and salts of iron made ready via distilled water. By the time, CTAB solution was also prepared. A clear CTAB solution was obtained by heating the solution on magnetic stirrer (hot plate) at 55°C . Stoichiometric volumes of salts solutions were then added in clear CTAB solution at $55\text{-}60^\circ\text{C}$. At this stage, NaOH solution was added in mixture to get a PH value of 11. After maintaining PH, mixture was further stirred for about 4 hrs. beakers were left un-disturbed until ferrite precipitates were settled down [8]. Continued periodic washing and draining was done to remove added NaOH content from the solution. Precipitates were washed again and again to neutralize the solution by lowering the PH value at 7. Excess water content was removed from precipitates by drying them in electric thermostatic oven at 95°C for 24 hrs [9]. Dried precipitates were then grinded in a fine mortar and pestle. Annealing of fine powdered samples was done in furnace at 850°C . Grinding was done again to get very fine and smooth powdered material. In the last, annealed and grinded nanoparticles were characterized through various methods to study their structural, morphological and magnetic properties [10].

XRD data for all six samples of $\text{LiCo}_{0.5}\text{Bi}_x\text{Fe}_{2-x}\text{O}_4$ ($0.00 < x < 0.25$ with 0.05 steps) was obtained through Netherlands, X'Pert Pro PAN Analytical with $\text{CuK}\alpha = 1.54 \text{ \AA}$. All samples were scanned for $2\theta = 20^\circ - 60^\circ$. SEM micrographs were obtained with different magnifications to estimate grain sizes and study surface properties and crystal structure. VSM was utilized to investigate the magnetic properties of freshly produced material at room temperature (298 K) [11].

3. Results and discussion

3.1. XRD analysis

X-ray diffractometer data of $\text{LiCo}_{0.5}\text{Bi}_x\text{Fe}_{2-x}\text{O}_4$ ($0.00 < x < 0.25$ with 0.05 steps) made ready through micro-emulsion route is plotted in a staked graph shown in (Figure. 1). Major prominent peaks appeared at about 30° , 35° , 42° and 57° . These diffraction angles correspond to the (202), (311), (400) and (333) lattice planes. The main peaks are identified as spinel structure of the $\text{LiCoFe}_2\text{O}_4$ and for further confirmation these peaks are verified by JCPDS card number 00-040-1119. These planes not only confirmed the formation of single phase but 311 peak is also a testimony of formation of cubic spinel phase as per expectations. There were less intense peaks

observed at about 32.5° and 49° which led to the proof of an orthophase formation as Bi₂O₃, these peak are identified using JCPDS# 00-006-0294 [12-14]

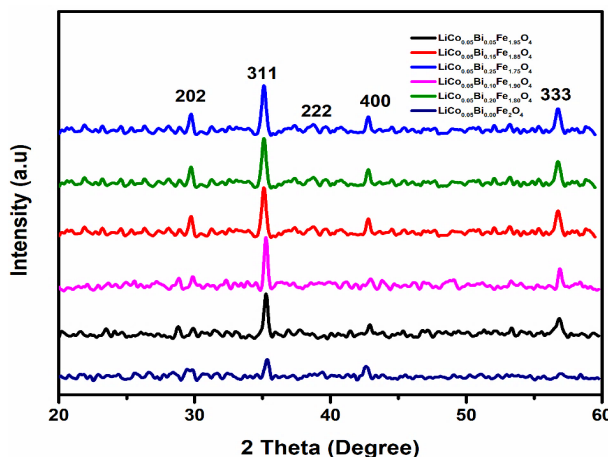


Fig. 1. XRD patterns of $\text{LiCo}_{0.5}\text{Bi}_x\text{Fe}_{(2-x)}\text{O}_4$ ($x = 0.00, 0.05, 0.10, 0.15, 0.20, 0.25$)

Crystal sizes were calculated via Debye Scherrer formula [15]:

$$D = \frac{k\lambda}{\beta \cos \theta} \quad (1)$$

where λ being the wave length of X-rays used, here Copper source is used with $K\alpha$ radiations of wave length 1.54 Å. ' k ' being the shape factor has a constant value of 0.9. ' β ' is the value of angle of the most intense, prominent peak with its full-width at half maximum commonly known as (FWHM). Calculations showed an increase in crystal sizes from 14 nm – 28 nm with increase in Bi⁺³ content is shown in (Figure. 2). Different ionic radii are responsible for variation in crystalline size and other structural parameters such as lattice parameters and unit cell volume. Increasing particle size was observed due to the higher tendency of agglomeration of larger ions in the parent lattice. Ionic radii are as Fe⁺³ = 0.645 Å, Co⁺² = 0.745 Å, Li⁺ = 0.76 Å, and Bi⁺³ = 1.03 Å. It is clear from $\text{LiCo}_{0.5}\text{Bi}_x\text{Fe}_{(2-x)}\text{O}_4$ that Li and Co are in fixed quantity so their effect cannot be compared and reported but amount of Fe is decreasing and Bi is increasing which is the actual reason for higher agglomeration as smaller Fe ions are replaced by the larger Bi ions that is why the particle size is increasing up to X = 0.25. This result is totally in agreement with our expectation of increase in crystal size due to the fact that substituting larger ion of bismuth is replacing smaller Fe⁺³ ions causing an increase in magnetic domains [16-19]. Lattice parameter ' a ' was calculated by [20]:

$$a = d\sqrt{h^2 + k^2 + l^2} \quad (2)$$

where ' d ' is the inter-planar distance which is found by using software X'Pert high score. hkl's are the miller indices of diffraction peaks. Lattice parameter also showed a little increase in value from 8.432 nm to 8.435 nm with the increase in concentration of bismuth is shown in (Figure. 3).

The following formula was used to compute X-ray density:

$$\rho = \frac{8M}{Na^3} \quad (3)$$

where ' ρ ' is the X-ray density, ' M ' is the molecular weight of the sample material, ' N ' is Avogadro number and ' a^3 ' is the cell volume. The density of X-ray was found increased with

increasing Bi^{+3} concentration is shown in (Figure. 3). The values of X-ray density are observed to lie between 6.38 to 6.88 (g / cm^3).

Dislocation density of the as prepared particles was calculated by the formula:

$$\delta = \frac{1}{D^2} \quad (4)$$

where, D is the crystallite size. Dislocation density was observed decreased with increasing Bi^{+3} content, which lies between 1.36 – 4.82 Lines / m^2 . Variations in dislocation density is shown in (Figure. 3). Lattice strain was calculated by Stokes-Wilson equation:

$$\varepsilon_L = \frac{\beta_{hkl}}{4 \tan \theta} \quad (5)$$

where, β is the Full width at half maxima. The microstrain was calculated by the following formula:

$$\varepsilon_L = \frac{\beta^* \cos \theta}{4} \quad (6)$$

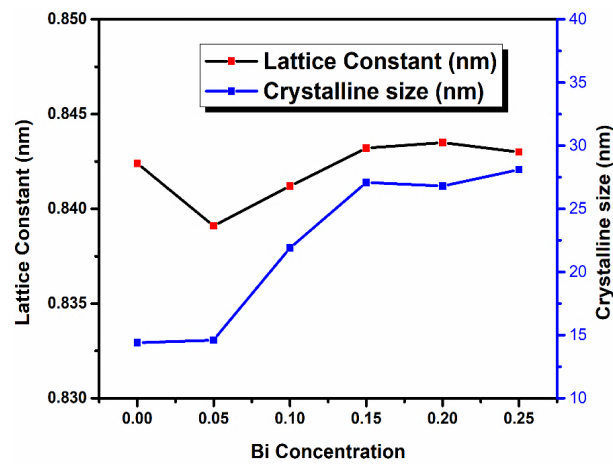


Fig. 2. Variation of lattice constant and crystalline size with Bi concentration.

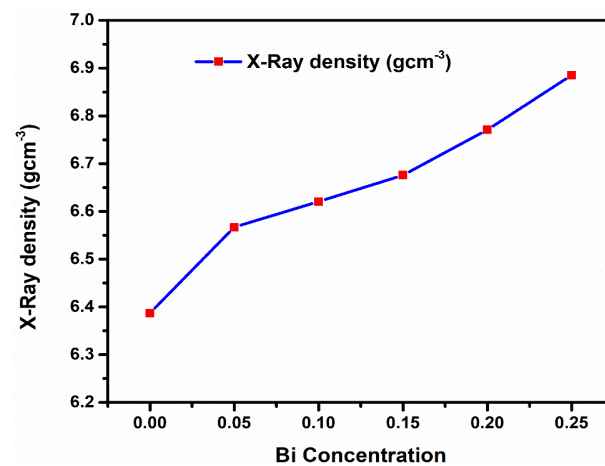


Fig. 3. Variation of X-ray density with Bi concentrations.

The lattice and microstrain shows variation with different Bi^{+3} concentration. The lattice strain was found to lie between 4.11 to 6.37×10^{-3} , while microstrain was found to lie $1.24 - 1.92 \times 10^{-3}$ ($\text{lines}^{-2}/\text{m}^{-4}$) as shown (Figure. 4).

Table 1. Lattice constant, Crystalline size, Cell volume and X-ray density for $\text{LiCo}_{0.5}\text{Bi}_x\text{Fe}_{(2-x)}\text{O}_4$ ($x = 0.00, 0.05, 0.10, 0.15, 0.20, 0.25$).

composition	Lattice constant a(nm)	Cell volume (nm^3)	X-ray density (gcm^{-3})	Crystalline size (nm)
X = 0.00	0.8424	0.5977	6.3873	14.4
X = 0.05	0.8391	0.5908	6.5667	14.6
X = 0.10	0.8412	0.5952	6.6205	21.9
X = 0.15	0.8432	0.5995	6.6757	27.09
X = 0.20	0.8435	0.6001	6.7706	26.8
X = 0.25	0.843	0.5990	6.8849	28.1

The XRD parameters of the nano-particles (Crystalline size, Lattice constant, X-ray and dislocation density, lattice and microstrain and the unit cell volume) with various dopant content ($x = 0.00, 0.05, 0.10, 0.15, 0.20, 0.25$) is tabulated in the (Table 1).

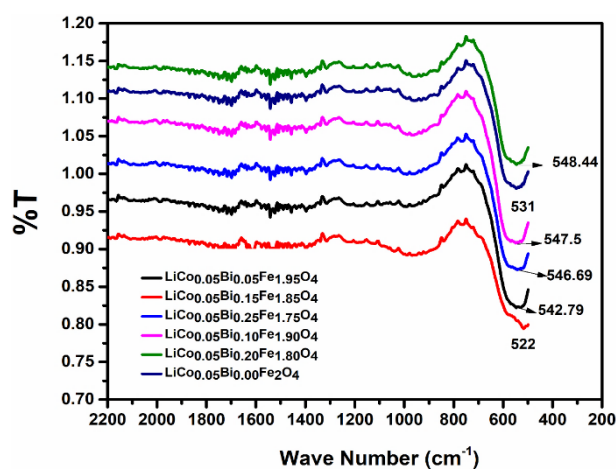


Fig. 4. FTIR spectrum for $\text{LiCo}_{0.5}\text{Bi}_x\text{Fe}_{(2-x)}\text{O}_4$ ($x = 0.00, 0.05, 0.10, 0.15, 0.20, 0.25$).

3.2. FTIR spectroscopic analysis

FTIR analysis showed maximum absorption at $531 - 548 \text{ cm}^{-1}$ for spectra's shown in (Figure. 4). These spectra's not only confirmed the creation of cubic spinel structure of all six prepared samples of $\text{LiCo}_{0.5}\text{Bi}_x\text{Fe}_{2-x}\text{O}_4$ ($0.00 < x > 0.25$ with 0.05 steps) but it also gave information about cation distribution and chemical changes involved. Two major frequency bands i.e. low frequency band around 400 cm^{-1} for vibrations at tetrahedral sites and high frequency band around $520-550 \text{ cm}^{-1}$ for vibrations at octahedral sides, must be there in FTIR spectra for the confirmation of spinel phase in under consideration samples, but in our present case of study, as the wave number range starts from 499 cm^{-1} so only tetrahedral sites vibrations can be seen clearly but they alone can be taken as clear indication of formation of single spinel phase in all compositions [21]. Here we are unable to calculate force constants for A-site and B-site as low frequency value is not available.

Table 2. FTIR absorption band values for $\text{LiCo}_{0.5}\text{Bi}_x\text{Fe}_{(2-x)}\text{O}_4$ ($0.00 < x < 0.25$).

Sr.No.	composition	$\nu(\text{cm}^{-1})$
1.	$\text{LiCo}_{0.5}\text{Bi}_{0.00}\text{Fe}_2\text{O}_4$	531
2.	$\text{LiCo}_{0.5}\text{Bi}_{0.05}\text{Fe}_{1.95}\text{O}_4$	522
3.	$\text{LiCo}_{0.5}\text{Bi}_{0.10}\text{Fe}_{1.90}\text{O}_4$	547.5
4.	$\text{LiCo}_{0.5}\text{Bi}_{0.15}\text{Fe}_{1.85}\text{O}_4$	542.79
5.	$\text{LiCo}_{0.5}\text{Bi}_{0.20}\text{Fe}_{1.80}\text{O}_4$	548.44
6.	$\text{LiCo}_{0.5}\text{Bi}_{0.25}\text{Fe}_{1.75}\text{O}_4$	546.69

However, shifting of high frequency value to even higher values with increasing Bi-content indicates a decrease in bond lengths at tetrahedral sites which in turn may lead us to expect an increasing strength of force constants [22-25]. The values of all these bands are tabulated in (Table 2).

3.3. SEM analysis

SEM micrographs of all prepared six samples $\text{LiCo}_{0.5}\text{Bi}_x\text{Fe}_{2-x}\text{O}_4$ ($0.00 < x < 0.25$ with 0.05 steps) showed cubical to spherical morphology of material particles which is in good connection with FTIR results confirming single phase spinel structure. Average estimated grain-size calculated from SEM micrographs is also in good agreement with particle size calculated from XRD data. Average size of 52 nm from SEM is actually a multiple of size of 18 nm - 28 nm as derived from XRD data which is attributed to the agglomeration of particles as shown in (Figure. 5) [26]. Nano-sized crystals leads to the confirmation of large surface-to-volume ratio. Larger surface areas indicated the applications of prepared materials in microwave devices [27-31].

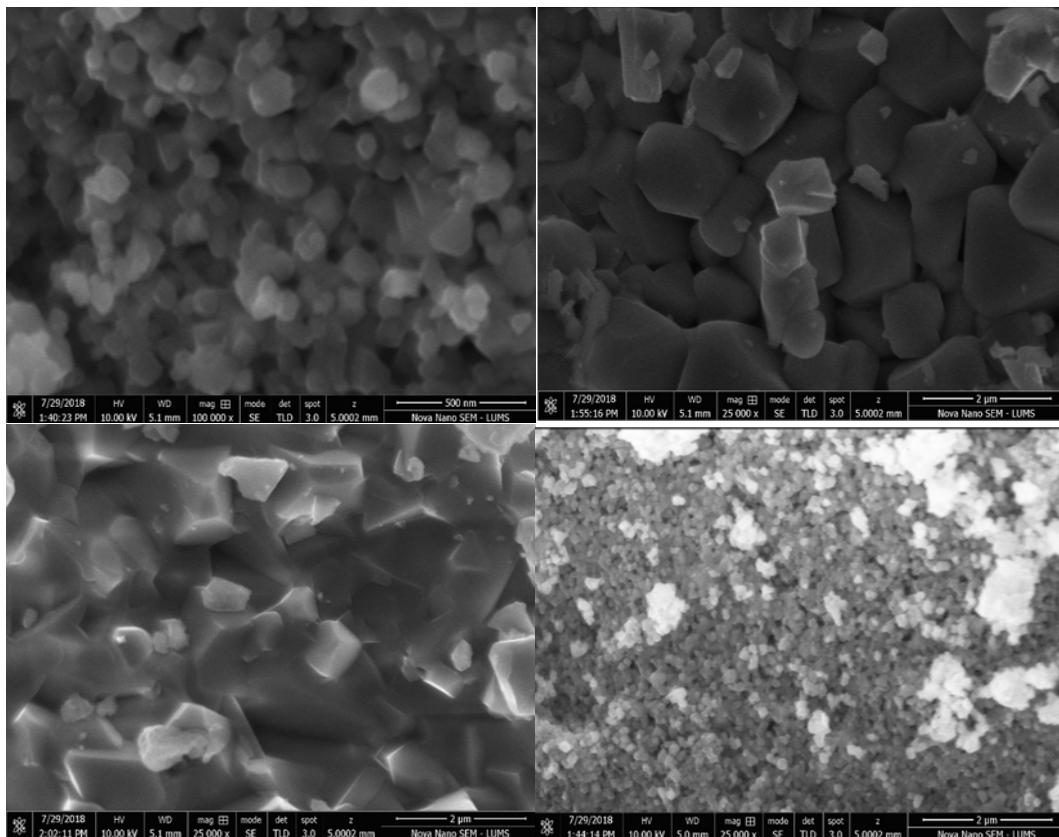


Fig. 5. SEM micrograph for $\text{LiCo}_{0.5}\text{Bi}_x\text{Fe}_{(2-x)}\text{O}_4$ ($x = 0.00, 0.1, 0.15, 0.20$).

3.4. VSM analysis

The hysteresis loops of Bi^{+3} doped Li–Co nanoparticles are shown in (Figure. 6). By the evidence of tinny loops of all the ready samples indicates that as prepared nanoparticles are the soft ferrites [32]. The Magnetic properties were calculated using loops of hysteresis, the results are given in (Table 3). VSM plots is shown in (Figure. 6), depicts the magnetic properties of synthesized ferrite magnetic materials at temperature of room (298K). M_s “saturation magnetization”, M_r “retentivity” and H_c “coercivity” values derived from M-H loop is shown in (Figure. 7). There was a decline in the number of M_s and M_r . The drop in M_s and M_r values might be attributed to bismuth's non-magnetic behavior and the displacement of Fe^{+3} ions from A-sites to B-sites by diamagnetic Bi^{+3} ions [32, 33].

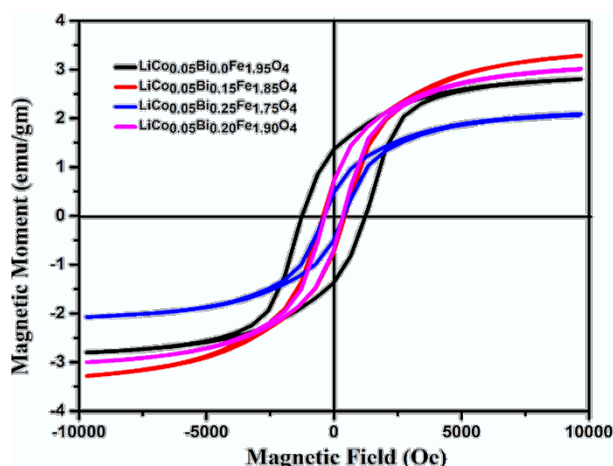


Fig. 6. Hysteresis loops curves for for $\text{LiCo}_{0.5}\text{Bi}_x\text{Fe}_{(2-x)}\text{O}_4$ ($x = 0.00, 0.15, 0.20, 0.25$) at room temperature (298 K).

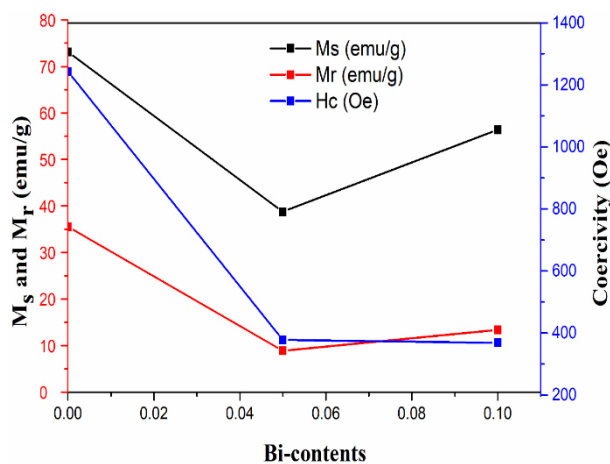


Fig. 7. Variation of M_s , M_r and H_c with Bi concentration ($x = 0.00, 0.15, 0.20$).

Saturation magnetization M_s reached its highest value of 73.12 (emu/g) at $x = 0.00$, whereas Retentivity M_r reached its maximum value of 35.54 (emu/g) at $x = 0.00$. The coercivity (H_c) of a magnetic material is an essential characteristic that is influenced by the anisotropic constant, saturation magnetization and crystalline size. With replacement of bismuth ions, the coercivity values showed a declining trend. Coercivity values are optimized via Bi^{+3} content doping, and the highest value is 1243.6 at $x = 0.00$ (Oe). At $x = 0.00$, the researchers discovered higher coercive force levels [34]. Because of their lower coercivity, these ferrites appear to be

good candidates for recording media applications. By addition of Bi^{+3} to the Li-Co nanoparticles, the values of the anisotropic constant falls. M_s and H_c are intimately connected to the anisotropy constant. This graph depicted the collective influence of these two parameters. The drop in the value of the anisotropy constant indicated a decrease in the value of coercivity. By a drop in domain-wall energy, the value of the anisotropic constant reduced [35].

Table 3. Magnetic properties of $\text{LiCo}_{0.5}\text{Bi}_x\text{Fe}_{(2-x)}\text{O}_4$ ($x = 0.00, 0.15, 0.20$).

composition	H_c (Oe)	M_s (emu/g)	M_r (emu/g)	M_s/M_r	Anisotropic constant
X = 0.00	1243.6	73.12	35.54	2.057	0.5582
X = 0.15	377.50	38.77	8.885	4.36	0.0898
X = 0.20	368.20	56.4	13.386	4.21	0.1274
X = 0.25	331.30	65.5	15.45	4.24	0.1283

4. Conclusions

$\text{LiCo}_{0.5}\text{Bi}_x\text{Fe}_{2-x}\text{O}_4$ ($0.00 < x < 0.25$ with 0.05 steps) have been prepared through microemulsion method. XRD studies revealed the formation of spinel ferrites. Lattice constant and crystalline size showed to be varied with increasing bismuth content. Crystalline size found to lie between 14 to 28 nm. Lattice parameters are calculated to be in nanometer scale. All XRD patterns confirmed the incorporation of Bi^{+3} as dopant without interrupting the uniform spinel structure of ferrites. SEM showed the somewhat cubical to spherical surface morphology of prepared samples confirming spinel structure. VSM analysis revealed the decreasing trend in both saturation magnetization and coercivity. A small value of anisotropic constant proves the newly synthesized material to be isotropic, thus expected to be good match for transformer cores.

Acknowledgements

The authors would like to acknowledge the Researcher's Supporting Project Number (RSPD2023R699) King Saud University, Riyadh, Saudi Arabia, for their support in this work.

References

- [1] A. Drmota, M. Drogenik, and A. Žnidaršič, *Ceramics International*, vol. 38, pp. 973-979, 2012; <https://doi.org/10.1016/j.ceramint.2011.08.018>
- [2] S. Bhukal and S. Singhal, *Materials science in semiconductor processing*, vol. 26, pp. 467-476, 2014; <https://doi.org/10.1016/j.mssp.2014.05.023>
- [3] A. Abbasi, H. Khojasteh, M. Hamadian, and M. Salavati-Niasari, *Journal of Materials Science: Materials in Electronics*, vol. 27, pp. 4972-4980, 2016; <https://doi.org/10.1007/s10854-016-4383-y>
- [4] A. Hajalilou, S. A. Mazlan, and K. Shamel, *Journal of physics and chemistry of solids*, vol. 96, pp. 49-59, 2016; <https://doi.org/10.1016/j.jpcs.2016.05.001>
- [5] M. Aghazadeh, I. Karimzadeh, and M. R. Ganjali, *Journal of Electronic Materials*, vol. 47, pp. 3026-3036, 2018; <https://doi.org/10.1007/s11664-018-6146-4>
- [6] R. Ali, M. A. Khan, A. Manzoor, M. Shahid, S. Haider, A. S. Malik, M. Sher, I. Shakir, and M. F. Warsi, *Journal of Magnetism and Magnetic Materials*, vol. 429, pp. 142-147, 2017; <https://doi.org/10.1016/j.jmmm.2017.01.007>
- [7] G. Aravind, M. Raghasudha, D. Ravinder, and R. V. Kumar, *Journal of Magnetism and Magnetic Materials*, vol. 406, pp. 110-117, 2016; <https://doi.org/10.1016/j.jmmm.2015.12.087>

- [8] H. M. N. u. H. Khan Asghar, M. K. Nawaz, R. Hussain, and Z. A. Gilani, *Journal of Materials and Physical Sciences*, vol. 1, pp. 98 - 108, 2020; <https://doi.org/10.52131/jmps.2020.0102.0010>
- [9] G. Nasar, H. Amin, F. Ahmad, and S. Nazir, *Journal of Materials and Physical Sciences*, vol. 1, pp. 19 - 25, 2020; <https://doi.org/10.52131/jmps.2020.0101.0003>
- [10] G. Nasar, I. Muhammad, F. Ahmad, S. Nazir, and F. ur Raheem, *Journal of Materials and Physical Sciences*, vol. 1, pp. 87 - 97, 2020; <https://doi.org/10.52131/jmps.2020.0102.0009>
- [11] S. Yasmeen, H. M. N. u. H. Khan Asghar, Z. A. Gilani, and K. Muhammad, *Journal of Materials and Physical Sciences*, vol. 1, pp. 26 - 36, 2020; <https://doi.org/10.52131/jmps.2020.0101.0004>
- [12] S. Bhukal, S. Mor, S. Bansal, J. Singh, and S. Singhal, *Journal of Molecular Structure*, vol. 1071, pp. 95-102, 2014; <https://doi.org/10.1016/j.molstruc.2014.04.073>
- [13] S. Bhukal, T. Namgyal, S. Mor, S. Bansal, and S. Singhal, *Journal of Molecular Structure*, vol. 1012, pp. 162-167, 2012; <https://doi.org/10.1016/j.molstruc.2011.12.019>
- [14] R. A. Bohara, N. D. Thorat, A. K. Chaurasia, and S. H. Pawar, *RSC Advances*, vol. 5, pp. 47225-47234, 2015; <https://doi.org/10.1039/C5RA04553C>
- [15] R. Cheruku, G. Govindaraj, and L. Vijayan, *Materials Research Express*, vol. 4, p. 125008, 2017; <https://doi.org/10.1088/2053-1591/aa9c2c>
- [16] M. A. Dar, J. Shah, W. Siddiqui, and R. Kotnala, *Journal of alloys and compounds*, vol. 523, pp. 36-42, 2012; <https://doi.org/10.1016/j.jallcom.2012.01.083>
- [17] N. Gupta, M. C. Dimri, S. C. Kashyap, and D. Dube, *Ceramics international*, vol. 31, pp. 171-176, 2005; <https://doi.org/10.1016/j.ceramint.2004.04.004>
- [18] N. Gupta, S. Kashyap, and D. Dube, *physica status solidi (a)*, vol. 204, pp. 2441-2452, 2007; <https://doi.org/10.1002/pssa.200622146>
- [19] M. J. Iqbal and M. R. Siddiquah, *Journal of Alloys and Compounds*, vol. 453, pp. 513-518, 2008; <https://doi.org/10.1016/j.jallcom.2007.06.105>
- [20] R. Kambale, P. Shaikh, C. Bhosale, K. Rajpure, and Y. Kolekar, *Smart Materials and structures*, vol. 18, p. 115028, 2009; <https://doi.org/10.1088/0964-1726/18/11/115028>
- [21] Z. A. Gilani, A. Farooq, N. u. H. K. Asghar, and M. Khalid, *Journal of Materials and Physical Sciences*, vol. 1, pp. 1 - 11, 2020; <https://doi.org/10.52131/jmps.2020.0101.0001>
- [22] M. Kaur and N. Kaur, *Ferrites and Ferrates: Chemistry and Applications in Sustainable Energy and Environmental Remediation*, ed: ACS Publications, 2016, pp. 113-136; <https://doi.org/10.1021/bk-2016-1238.ch004>
- [23] K. K. Kefeni, T. A. Msagati, and B. B. Mamba, *Materials Science and Engineering: B*, vol. 215, pp. 37-55, 2017; <https://doi.org/10.1016/j.mseb.2016.11.002>
- [24] V. S. Kiran and S. Sumathi, *Journal of Magnetism and Magnetic Materials*, vol. 421, pp. 113-119, 2017; <https://doi.org/10.1016/j.jmmm.2016.07.068>
- [25] V. S. Kirankumar and S. Sumathi, *Journal of Materials Science: Materials in Electronics*, vol. 29, pp. 8738-8746, 2018; <https://doi.org/10.1007/s10854-018-8890-x>
- [26] G. Nasar, U. Khalil, M. S. Khan, and Q. Nadeem, *Journal of Materials and Physical Sciences*, vol. 3, pp. 14 - 21, 2022; <https://doi.org/10.52131/jmps.2022.0301.0022>
- [27] K. V. Kumar and N. S. Kumar, *Materials Today: Proceedings*, vol. 3, pp. 4193-4198, 2016; <https://doi.org/10.1016/j.matpr.2016.11.095>
- [28] M. Pal, P. Brahma, and D. Chakravorty, *Journal of magnetism and magnetic materials*, vol. 152, pp. 370-374, 1996; [https://doi.org/10.1016/0304-8853\(95\)00483-1](https://doi.org/10.1016/0304-8853(95)00483-1)
- [29] P. Pandya, H. Joshi, and R. Kulkarni, *Journal of materials science*, vol. 26, pp. 5509-5512, 1991; <https://doi.org/10.1007/BF02403950>
- [30] K. Praveena and S. Srinath, *Advanced Science, Engineering and Medicine*, vol. 6, pp. 359-365, 2014.
- [31] R. Waldron, *Physical review*, vol. 99, p. 1727, 1955; <https://doi.org/10.1103/PhysRev.99.1727>
- [32] S. Zare, A. A. Ati, S. Dabagh, R. Rosnan, and Z. Othaman, *Journal of Molecular Structure*,

- vol. 1089, pp. 25-31, 2015; <https://doi.org/10.1016/j.molstruc.2015.02.006>
- [33] K. Maaz, A. Mumtaz, S. Hasanain, and M. Bertino, *Journal of Magnetism and Magnetic Materials*, vol. 322, pp. 2199-2202, 2010; <https://doi.org/10.1016/j.jmmm.2010.02.010>
- [34] N. Rezlescu and E. Rezlescu, *physica status solidi (a)*, vol. 23, pp. 575-582, 1974; <https://doi.org/10.1002/pssa.2210230229>
- [35] S. E. Shirsath, M. L. Mane, Y. Yasukawa, X. Liu, and A. Morisako, *Physical Chemistry Chemical Physics*, vol. 16, pp. 2347-2357, 2014; <https://doi.org/10.1039/C3CP54257B>